Jiniraj et al. 2021. *Int. J. Vehicle Structures & Systems*, 13(1), 91-96
ISSN: 0975-3060 (Print), 0975-3540 (Online)
doi: 10.4273/ijvss.13.1.18

International Journal of Vehicle Structures & Systems
Available online at www.maftree.org/eja

Leading Edge Shape Optimization of Whitcomb IL Airfoil in Transonic Flow using a Multi-Objective Genetic Algorithm

R. Jiniraj[a], T. Logesh[b] and D. Rajapatel[c]

Dept. of Aeronautical Engg., Er. Perumal Manimekalai College of Engg., Tamil Nadu, India
[a]Corresponding Author, Email: jinirajaero@gmail.com
[b]Email: logesh99t@gmail.com
[c]Email: d.rajapatel19989@gmail.com

ABSTRACT:

Leading edge shape optimization of transonic airfoils requires creating an airfoil surface that reduces the drag divergence due to transonic shocks by either delaying them or reducing their strength at a given transonic cruise speed while maintaining the lift. Aircrafts like Boeing 757, Airbus A300, Boeing 777 and McDonnell Douglas AV-8B Harrier II use Whitcomb IL supercritical airfoil for efficient aerodynamic performance in transonic conditions. This study employs a multi-objective genetic algorithm (MOGA) for shape optimization of leading edge of the Whitcomb IL airfoil to achieve three objectives, namely dilation of shock, reduction in leading edge radius and increment of lift at a given transonic Mach number and at the given angle of attack. The commercially available software ICEM CFD and Fluent are employed for calculation of the flow field using the Reynolds-averaged Navier-Stokes equations (RANS) in conjunction with a two equation turbulence model. It is shown that the MOGA can generate superior airfoil compared with Whitcomb IL airfoil by achieving three objectives. The optimized airfoil configuration is validated by wind tunnel testing facility.

KEYWORDS:

Leading edge; Whitcomb IL airfoil; Reynolds-averaged Navier-Stokes; Multi-objective genetic algorithm

CITATION:

R. Jiniraj, T. Logesh and D. Rajapatel. 2021. Leading Edge Shape Optimization of Whitcomb IL Airfoil in Transonic Flow using a Multi-Objective Genetic Algorithm, *Int. J. Vehicle Structures & Systems*, 13(1), 91-96. doi:10.4273/ijvss.13.1.18.

1. Introduction

Usually modern commercial aircrafts operate at transonic cruise speeds. Therefore, in recent years, the shape optimization of an aircraft at transonic speeds to minimize the shock drag has become a topic of great interest in computational aerodynamics [1-3]. An aircraft in motion at transonic speeds run into a speedy increase in drag due to the shock waves performing on various locations on its surface, mainly on the wings. These shock waves cause flow variability and increase in drag force, which result in higher fuel consumption or reduced energy efficiency. Therefore, the goal of shape optimization is to design shock-free airfoils or dilation of shock wings to reduce shock drag. However, the drag reduction alone cannot be the optimization goal if it can undesirably affect the lift; in general, there is a balance between lift and drag [4]. Several important criteria must be met in the optimization process to achieve not only a dilation of shock but also an efficient airfoil that has good drag characteristics, a batter boundary high enough to permit cruising at design lift coefficient, no poor off-design performance, and so forth [5].

In the last several decades, many important contributions have been made to the design and optimization of shock-free Airfoils. In the late 1950s, Morawetz [6] determined that shock-free airfoil and dilation of shock airfoil are special remote solutions and a small perturbation from them would cause the appearance of a shock. In 1960s, Whitcomb and Clark [7] developed their famous supercritical airfoils for transonic flow and Garabedian and Korn [8] developed the successful method of complex characteristics in the hodograph plane for obtaining shock-free airfoils and dilation of shock. Using the hodograph method, Nieuwland [9] reported shock-free transonic flows around quasi elliptical Airfoils sections in 1967. The goal of this article is to employ a multi objective genetic algorithm (MOGA) for shape optimization of some well-known airfoils [10], namely the Whitcomb-IL airfoil, at transonic speed to improve their aerodynamics characteristics, which is to reduce their drag by achieving shock-free shapes as well as to maintain or increase their lift.

2. Genetic algorithm

Multi objective optimization is a method of finding optimum solutions of problems with two or more objectives. Using the multi objective optimization, shape optimization and optimization of aerodynamic parameters is done for Whitcomb IL airfoil. In this study, the MOGA algorithm is employed to find the Pareto-optimal solutions to the airfoil optimization problem [11-19]. The most commonly known Non-

Dominated Sorting Genetic Algorithm II is used. In NSGA-II, a Pareto-optimal solution set is defined such that any individual inside the set dominates any individual outside the set while any individual in the set is not dominated by another individual in the solution set. Here, a feasible solution x is said to dominate another feasible solution y, if and only if all the objectives of x are not worse than those of y and at least one objective of x is better than that of y. A solution is said to be Pareto-optimal if it is not dominated by any other solution in the solution.

3. Parameterization of Whitcomb IL airfoil

The airfoil shapes are parameterized using Bezier curves. Bezier curves are parametric curves frequently used in computer graphics and relate fields [20-26]. A Bezier curve is defined by a set of Bezier control points. Each curve can be expressed as math equations containing the information of Bezier control points. The number of points required to parameterize a curve depends on the shape of the curve. In this study control points are chosen from 15-20% chord from the leading edge. Totally 15 control points are chosen for parameterization on the upper and lower surface of the airfoil. The AoA is defined as follows,

$$\alpha = \alpha_{base} - \alpha_{Clo} \quad (1)$$

Through convergence analyses, optimization runs were performed with a suitable number of generations and population size. Each optimization was repeated to verify that consistent findings were achieved. Since the aerodynamic characteristics of each airfoil were mostly studied in this work, the aerodynamically best performance airfoil from each Javafoil theory front of solutions was used for all comparisons.

4. Algorithm implementation

This topic describes the computational setup. Fig. 1 schematically illustrates how MOGA interfaces with the external mesh generator Javafoil and CFD solver Fluent. Javafoil already yields sufficient accuracy of the results. Since the MOGA involves fitness evaluation for a large number of airfoils with various shapes, we are using 15 control points for both the top and bottom surface, thus the degree of the Bezier curve is 7. For an airfoil curve, the first point and the last two points are fixed since they represent the leading and trailing edge of the airfoil. The intermediate points are allowed to move within the boundaries. At the top surface, 7 control points Point 1 (x1, y1), Point 2 (x2, y2), Point 3 (x3, y3), Point 4 (x4, y4), Point 5 (x5, y5), Point 6 (x6, y6) and Point 7 (x7, y7) are used.

At the bottom surface, 7 control points Point 1' (m1, n1), Point 2' (m2, n2), Point 3' (m3, n3), Point 4' (m4, n4), Point 5' (m5, n5), Point 6' (m6, n6) and Point 7' (m7, n7), are employed. The constraints applied to the Bezier control points are shown in Table 1. The implementation of MOGA involves the following steps. At the initial condition MOGA generates a number of individuals according to the generation size. Since each individual represents one feasible airfoil, the airfoil has Bezier base points. The generated airfoils are shown in Fig. 1, Fig. 2 and Fig. 3.

Table 1: Bezier control points and their lower/upper bounds used for airfoil shape optimization in MOGA

Airfoil	Beizer coordinates	Whitcomb IL	
		Base airfoil bound	Optimized airfoil bound
Top surface	x1	0.0003	0.0003
	x2	0.0021	0.0024
	x3	0.0075	0.0088
	x4	0.0194	0.0228
	x5	0.0409	0.048
	x6	0.0745	0.0874
	x7	0.1224	0.1428
	y1	0.0034	0.0011
	y2	0.0096	0.0032
	y3	0.0176	0.0083
	y4	0.0253	0.015
	y5	0.0324	0.0235
	y6	0.0393	0.0337
	y7	0.0453	0.0454
Bottom surface	m1	0.0003	0.0003
	m2	0.002	0.0024
	m3	0.0075	0.0088
	m4	0.0194	0.0228
	m5	0.0408	0.0479
	m6	0.0745	0.0873
	m7	0.1223	0.1427
	n1	-0.0033	-0.0013
	n2	-0.0095	-0.0047
	n3	-0.0176	-0.0093
	n4	-0.0255	-0.0165
	n5	-0.0334	-0.0247
	n6	-0.0407	-0.0342
	n7	-0.0469	-0.0453

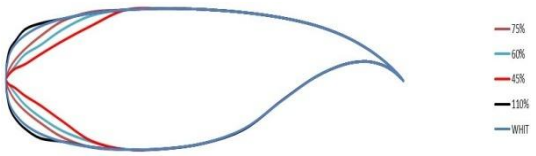

Fig. 1: Different thickness edge thickness of Whitcomb airfoil

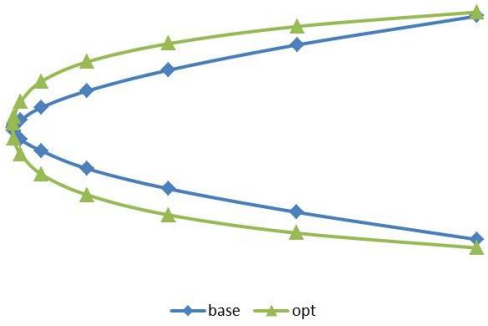

Fig. 2: Bezier curves and Bezier control points

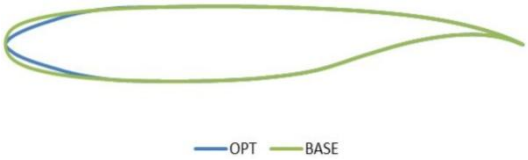

Fig. 3: Whitcomb IL vs. optimized final airfoil

Using MOGA procedure as outlined in Fig. 4, the optimized airfoil compared with Whitcomb IL airfoil are shown in Fig. 3. The evaluation of aerodynamic performance was varied between C_l/C_d at angles of attack (AOA) denoted as $\alpha = 6^o \pm 3$ to account for wind gusts and off-design conditions. Since this study is solely focused on the optimization of the airfoil itself, and not the airfoil design, the influential effects of leading edge on the airfoil optimization results were eliminated by formulating all aerodynamic evaluations relative to the zero-lift AoA (α_{Clo}). This step describes the investigation of aerodynamic flow field using Javafoil and ICEM CFD computation. The CFD simulation is carried out using ANSYS Fluent [27]. Spallart Allmaras equation model is selected to solve the turbulent flow conditions [28].

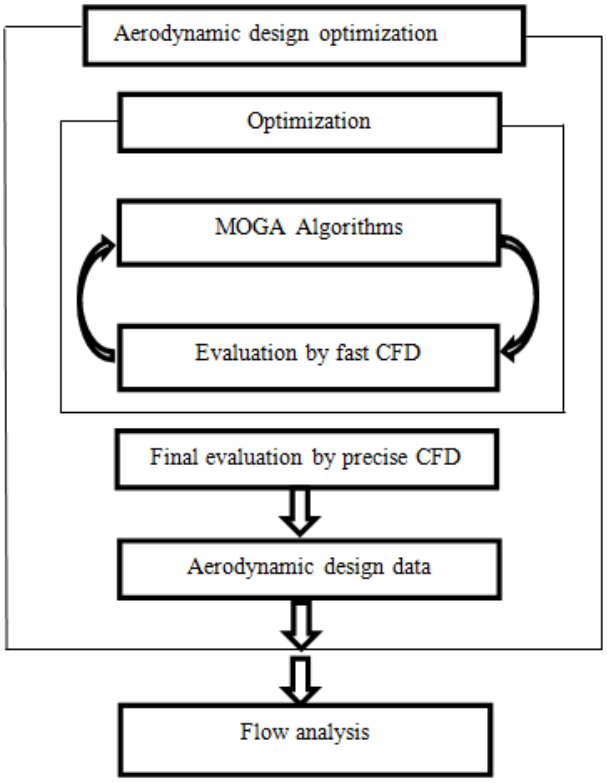

Fig. 4: Diagram of information flow in MOGA

5. Mesh study

Figs. 5 and 6 show the mesh of the airfoil with C-domain. The mapped meshing is created on entire domain. The cross section is developed to be fine at areas near to the airfoil and coarser more remote far from the airfoil. For this airfoil a quadratic element was utilized. The mesh has to be fine also in certain regions far from airfoil. Mesh study is carried out to reduce the influence of number of grids on the computational results. It shows how the solutions changes little when spacing is changed. Fig. 7 shows the variation of C_l when the wall spacing is changed. From the plot it is clear that the value of C_l for Δs/1 is more when compared to the results obtained from different values of wall spacing. So wall spacing of Δs = 1.73691089401 $e^{-1}m$ is selected for computation. Table 2 shows the aerodynamic coefficients obtained for different wall spacing with converged and un-converged iterations.

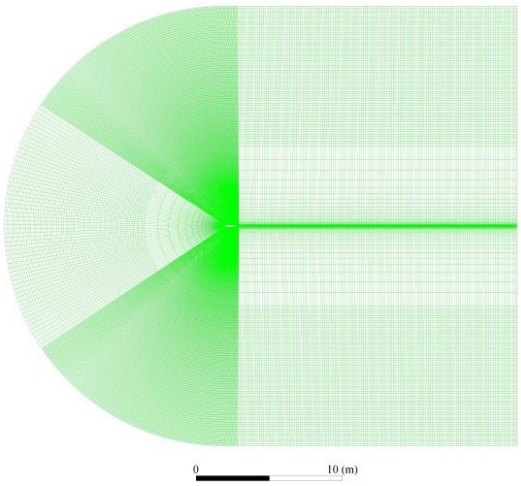

Fig. 5: Mesh of optimised airfoil

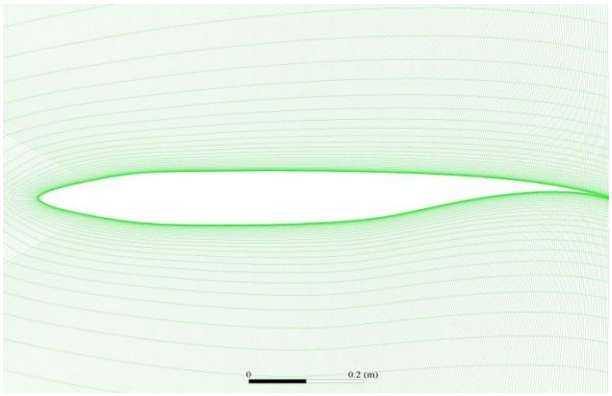

Fig. 6: Fine mesh around airfoil surface

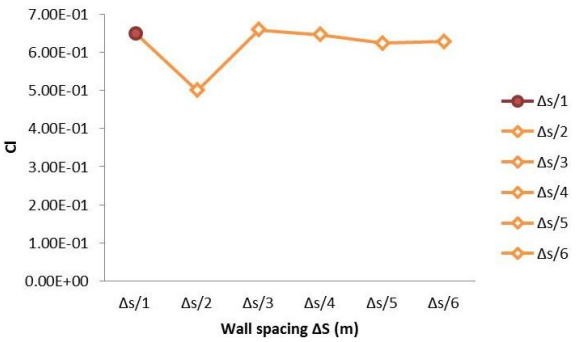

Fig. 7: Grid independence study

Table 2: Mesh study

ΔS	C_l	C_d	Iteration
Δs/1	6.49E-01	1.56E-02	Converged
Δs/2	5.00E-01	1.96E-02	Converged
Δs/3	6.59E-01	2.06E-02	Converged
Δs/4	6.46E-01	3.46E-02	Un-converged
Δs/5	6.24E-01	1.45E-02	Un-converged

6. Results and discussion

The lift coefficient is a dimensionless number that establishes a relationship between the lift generated by lifting body to fluid properties around the body. The lift coefficient is defined by,

$$Cl = L/qS \quad (2)$$

Where, q = dynamic pressure. Fig. 8 shows the variation of lift of Whitcomb IL airfoil and optimized Whitcomb IL airfoil with different degrees of AoA. From the plot it

is evident that the value of lift with increasing AoA. Up to 1° AoA the C_l value is decreasing for Whitcomb IL airfoil. After 1° AoA, there is a gradual increase in C_l value with increase in AoA the maximum value of C_l obtained is about 1.8° at 10° AoA. Also, the variation of lift coefficient of optimized airfoil with AoA is plotted. At 0° AoA the value of lift coefficient is almost 1 for optimized airfoil. There is a slight increase in C_l at 0° AoA. Due to the optimized shape at leading edge, C_l value is increasing at lower AoA than Whitcomb IL airfoil. By increasing the AoA, C_l value increasing far better than the Whitcomb IL airfoil. Therefore, optimized Whitcomb IL produces better lift coefficient when compared with Whitcomb IL airfoil.

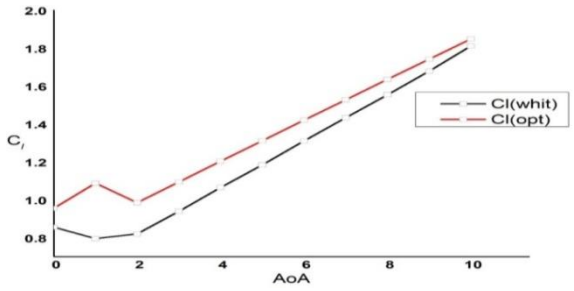

Fig. 8: Cl vs. AoA for Whitcomb IL and optimized airfoil

The drag coefficient is the dimensionless number used to indicate the resistance of an object in a fluid. Fig. 9 indicates the variation of drag coefficient of Whitcomb IL airfoil and optimized Whitcomb IL for different AoA from 0 to 12 degrees. For Whitcomb IL airfoil, the value of drag at 0° AoA is about 0.07 and the value of drag decreases abruptly at 1° AoA. Then there is linear increase in drag with increasing AoA and the maximum value of drag obtained is about 0.15 at 1**0**° AoA. In the plot, the value of drag at 0° AoA is about 0.03 and the value of drag decreases to 0.025 at 1° AoA. Then there is increase in drag with increasing AoA but the drag is very low for all AoA as compared with the Whitcomb IL airfoil. The maximum value of drag obtained is about 0.06 at 10° AoA which is very much lesser value when compared to the drag obtained by Whitcomb airfoil. Thus morphing airfoil produces optimum performance [28, 29].

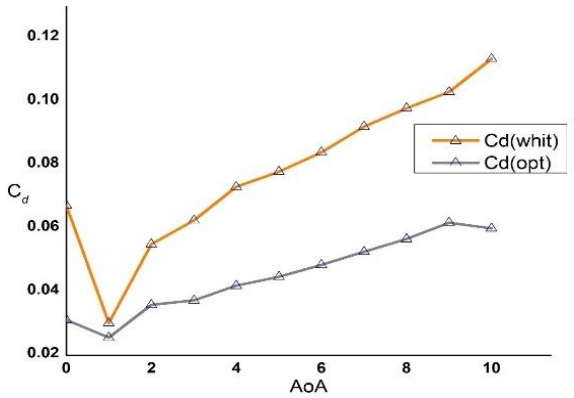

Fig. 9: C_d vs. AoA for Whitcomb IL and optimized airfoil

Fig. 10 shows the variation of lift to drag ratio with AoA. From the graph it is evident that the value of C_l/C_d at 0° AoA is about 13 and it increases sharply at 1° AoA which shows that there is large lift generated with minimal drag. The value of C_l/C_d is almost constant for AoA from 2° to10°. The value of lift drag ratio at 0° AoA is about 30, which is high compared to the Whitcomb IL airfoil. When the AoA is increased further beyond 3°, the optimized airfoil shows better performance than Whitcomb IL airfoil. Table 3 shows that the relative improvement in the properties of optimized airfoils compared with the original airfoils.

Table 3: Improvement in aerodynamic parameters

M	α, °	Optimized airfoil			Whitcomb IL airfoil		
		C_l	C_d	$C_l/_d$	C_l	C_d	C_l/C_d
0.73	0	0.955	0.031	30.64	0.855	0.067	12.72
0.73	2	0.984	0.035	27.40	0.872	0.056	15.379
0.75	2.8	1.127	0.048	23.10	0.932	0.063	14.702
0.75	2	1.035	0.035	29.35	0.898	0.061	14.542
0.8	1.5	0.967	0.038	24.99	0.786	0.060	20.098

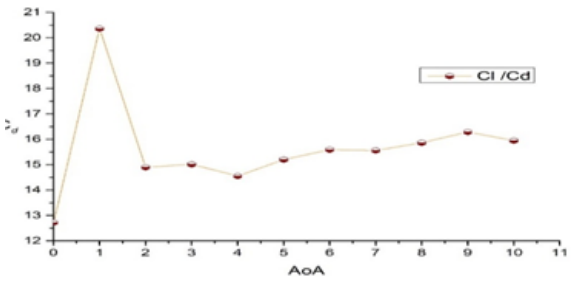

Fig. 10(a): C_l/C_d vs. AoA (Whitcomb IL airfoil)

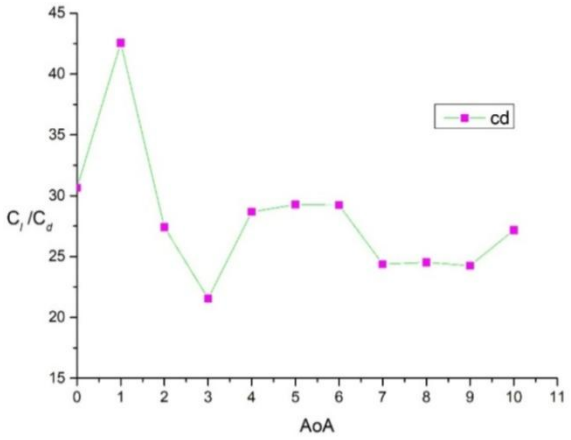

Fig. 10(b): C_l/C_d vs. AoA (Optimized airfoil)

Fig. 11 shows the variation of lift coefficient of Whitcomb IL airfoil and optimized airfoil with AoA. There are different optimized airfoils indicated by 50%, 55%, 58%, 60% and 75%. It is clearly evident that airfoil with 75% optimization yields the best result. So the leading edge of Whitcomb IL airfoil is optimized to 75% to yield the best aerodynamic properties. The most important parameter to determine aerodynamic performance is C_p contour plot. The C_p for both Whitcomb IL airfoil and optimized airfoil is displayed in Fig. 12. Black color dots indicate the C_p of Whitcomb IL airfoil. Red color indicates the C_p contour for optimized airfoil. The difference between the upper and lower surface C_p is responsible for the lift and drag on the surface of the airfoil. In this plot, the C_p is plotted against the chord of the airfoil. The max C_p of Whitcomb IL airfoil is around 1.2 and the minimum value is around -1.2. But for optimized airfoil, the maximum C_p value is

around 1.2 and minimum value is around -1.7. This shows that optimized airfoil decreases drag and improves lift and produces better performance compared with Whitcomb IL airfoil.

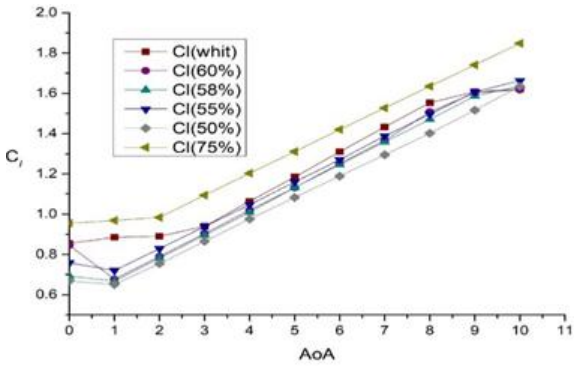

Fig. 11: Selection of optimized percentage airfoil

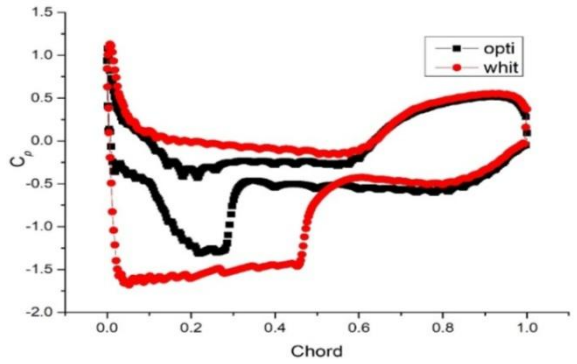

Fig. 12: Cp contour - Whitcomb IL airfoil vs. Optimized airfoil

7. Flow field analysis

The velocity contour for both Whitcomb IL and optimized airfoil at M = 0.73, AoA = 0° is shown in Fig. 13 and Fig. 14 respectively. The lift and drag are proportional to the velocity of air around the airfoil. Shock is started to arise at the top of the Whitcomb IL airfoil section. The same condition is checked for the optimized airfoil. It is clear from the contour (Fig. 14) that the shock formation is delayed somewhat and makes this optimized airfoil better to choose for transonic airplanes. The aerodynamic performance is enhanced for optimized airfoil than Whitcomb IL airfoil.

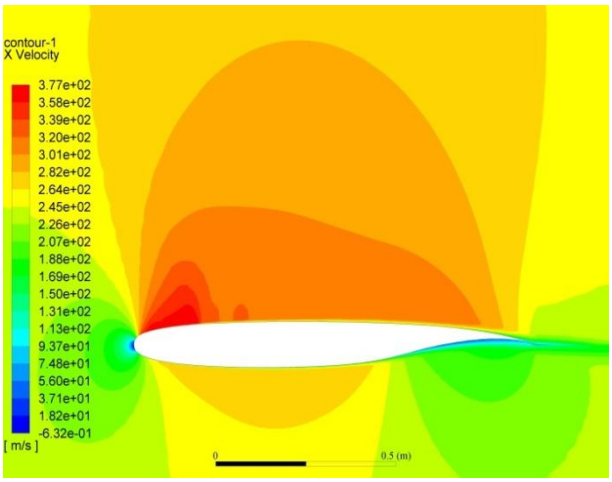

Fig. 13: Velocity field at M = 0.73, AoA = 0° - Whitcomb IL airfoil

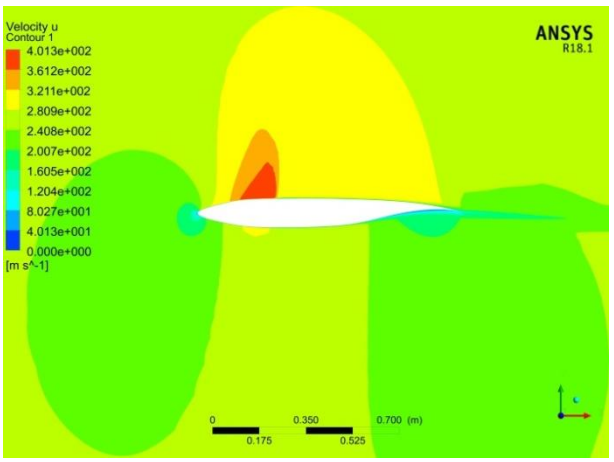

Fig. 14: Velocity field at M = 0.73, AoA = 0° - Optimized airfoil

8. Conclusion

This study has made several important contributions to the study of airfoil optimization. It is shown that Genetic algorithm technique can be employed efficiently and accurately to produce generally optimal airfoils with good aerodynamic properties using a desired objectives of Cd and/or Cl/Cd. In addition, this study has verified that the application of multi-objective algorithm can result in superior shock delay airfoils by reducing the drag and get the most out of the lift to drag ratio.

REFERENCES:

[1] L.D. Huff. 1987. Analysis of viscous transonic flow over airfoil sections, *NASA Tech. Memorandum 88912*.

[2] K. Zaman and D. Mckinzie. 1989. Control of laminar separation over airfoils by acoustic excitation, *Proc. 27th Aerospace Sci. Meeting*, Reno, Nevada, U.S.A. https://doi.org/10.2514/6.1989-565.

[3] M. Drela and M.B. Giles. 2012. Viscous-inviscid analysis of transonic and low reynolds number airfoils, *AIAA J.*, 25(10), 1347-1440. https://doi.org/10.2514/3.9789.

[4] A. Jameson. 2003. CFD for aerodynamic design and optimization, its evolution over the last three decades, *Proc. 16th AIAA Computational Fluid Dynamics Conf.*, USA. https://doi.org/10.2514/6.2003-3438.

[5] M. Harbeck and A. Jameson. 2005. Exploring the limits of shock-free transonic airfoil design, *Proc. 43rd Aerospace Sci. Meeting and Exhibit*, USA. https://doi.org/10.2514/6.2005-1041.

[6] K. Leoviriyakit and A. Jameson. 2005. Multi-point wing plan form optimization via control theory, *Proc. 43rd AIAA Aerospace Sci. Meeting & Exhibit*, USA. https://doi.org/10.2514/6.2005-450.

[7] S. Obayashi, A. Oyama and T. Nakamura. 2000. Transonic wing shape optimization based on evolutionary algorithms, *Proc. 3rd Int. Symp. High Performance Computing*, Japan.

[8] R.T. Whitcomb and L.R. Clark. 1965. *An Airfoil Shape for Efficient Flight at Supercritical Mach Numbers*, NASA Report No - TM X-1109.

[9] P.R. Garabedian and D.G. Korn. 1971. Analysis of transonic airfoils, *Communications on Pure and Applied Mathematics*, 24, 841-851. https://doi.org/10.1002/cpa.3160240608.

[10] G.Y. Nieuwland. 1967. *Transonic Potential Flow Around a Family of Quasi-Elliptical Aerofoil Sections*, National Aerospace Lab. NLR, Report No. - TR-T172.

[11] *NACA Airfoil Series*. http://www.aerospaceweb.org/question/airfoils/q0041.shtml.

[12] C.D. Ronco and E. Benini. 2013. A simplex crossover based evolutionary algorithm including the genetic diversity as objective, *Applied Soft Computing*, 13(4), 2104-2123. https://doi.org/10.1016/j.asoc.2012.11.003.

[13] L. Padovan, V. Pediroda and C. Poloni. 2003. Multi objective robust design optimization of airfoils in transonic field, *Proc. Int. Congress on Evolutionary Methods for Design, Optimization and Control with Applications to Industrial Problems*, Spain.

[14] D.E. Goldberg. 1989. *Genetic Algorithms in Search, Optimization & Machine Learning*, Addison-Wesley Professional, 1st Ed.

[15] N. Srinivas and K. Deb. 1994. Multi-objective function optimization using non-dominated sorting genetic algorithms, *Evolutionary Computation*, 2(3), 221-248. https://doi.org/10.1162/evco.1994.2.3.221.

[16] A. Konak, D.W. Coit and A.E. Smith. 2006. Multi-objective optimization using genetic algorithms - A tutorial, *Reliability Engg. and System Safety*, 9, 992-1007. https://doi.org/10.1016/j.ress.2005.11.018.

[17] K. Deb. 2004. Single and multi-objective optimization using evolutionary computation, *Proc. 6th Int. Conf. Hydro-Informatics*, Singapore. https://doi.org/10.1142/9789812702838_0003.

[18] A.D. Gaspari and S. Ricci. 2015. Knowledge-based shape optimization of morphing wing for more efficient aircraft, *Int. J. Aerospace Engg.*, Article No - 325724. https://doi.org/10.1155/2015/325724.

[19] B. Yang, Q. Xu, L. He, L.H. Zhao, Ch.G. Gu and P. Ren. 2015. A novel global optimization algorithm and its application to airfoil optimization, *J. Turbo Machinery*, 137(4), Article No - 041011. https://doi.org/10.1115/1.4028712.

[20] J.A. Reuther, A. Jameson, J.J. Alonso, M.J. Rimlinger, and D. Saunders. 1999. Constrained multipoint aerodynamic shape optimization using AD joint formulation and parallel computers, *AIAA J.*, 36(1), 51-74. https://doi.org/10.2514/2.2413.

[21] R. Bettadapura, T. Mashburn and R. Crawford. 2013. *Length Constrained Bezier Curve Smoothing*, Corpus id: 7515545.

[22] S. Ameduri. 2018. Chapter 16 - Morphing of the Leading Edge, *Morphing Wing Tech.*, 491-515. https://doi.org/10.1016/B978-0-08-100964-2.00016-2.

[23] A. Magrini and E. Benini. 2018. Aerodynamic optimization of a morphing leading edge airfoil with a constant arc length parameterization, *J. Aerospace Engg.*, 31(2). https://doi.org/10.1061/(ASCE)AS.1943-5525.0000812.

[24] Z. Lyu and J.R.R.A. Martins. 2015. Aerodynamic shape optimization of an adaptive morphing trailing edge wing, *J. Aircraft*, 52, 1951-1970.

[25] J.A. Samareh. 1999. A survey of shape parameterisation techniques, *Int. Forum on Aero Elasticity and Structural Dynamics*, NASA, Hampton, VA, USA.

[26] B.M. Kulfan. 2007. CST universal parametric geometry representation method with application to supersonic aircraft, *Proc. 4th Int. Conf. on Flow Dynamics*, Japan. https://doi.org/10.2514/6.2007-62.

[27] M. Secanell, A. Suleman and P. Gamboa. 2006. Design of a morphing airfoil using aerodynamic shape optimization, *AIAA J.*, 44, 1550-1562. https://doi.org/10.2514/1.18109.

[28] S.R. Allmaras and F.T. Johnson. 2012. Modifications and clarifications for the implementation of the Spalart-Allmaras turbulence model, *Proc. 7th Int. Conf. Computational Fluid Dynamics*, USA.

[29] H. Suzuki, K. Rinoie and A. Tezuka. 2010. Laminar airfoil modification attaining optimum drag reduction by use of airfoil morphing, *J. Aircraft*, 47(4), 1126-1132. https://doi.org/10.2514/1.46152.